From Particle Dimensions to Electron Motion and Hydrogen Spectral Structure

A Four-Spatial-Dimensional IDWT Construction

Fedge No
Independent researcher
fedge-no@hotmail.com

8 November 2026 — Version 2.2

Abstract

We present the successful mathematical and numerical results of a trajectory-led investigation of hydrogen within Infinite Dimensional Wave Theory. Starting with the particle-depth picture, a four-real-coordinate electron orbit yields exact rotation/precession components $|\delta - \beta|$ and $\delta + \beta$. The component ratios, whole-frequency patterns, and energy sequences follow from the stated equations. An absolute calculation using electron mass and specified hydrogen energy and radius scales gives an ultraviolet component at 101.91 nm without tuning a wavelength, approximately 0.65% from Lyman-β. The complete pattern $(1, 2, 3, 4)$ has seven exact placements in the gross hydrogen spectrum through upper level 100 and an octave chain through level 200. The supplied orbit-action family contains the square energy sequence $(1, 4, 9, 16)$, with 43 exact placements through level 100 and 147 through level 200. We give the derivations, all level-100 assignments, exact octave identities, and reproducible checks. A separate anisotropic nuclear-potential calculation generates precession dynamically. The account follows the successful progression and identifies what the results calculate: trajectory geometry, energy relations, gross spectral correspondences, and conditional precession dynamics. These do not yet constitute a complete derivation of hydrogen's selected states or optical strengths.

Keywords: hydrogen spectrum; deterministic electron trajectories; four spatial dimensions; precession; Rydberg formula; exact frequency ratios; octave scaling; Infinite Dimensional Wave Theory.

Contents

1 How the investigation developed **3**

2 Distinctions from earlier atomic models **4**

3 The question and the result **4**

4 Physical scope and notation **5**

5 The trajectory and its exact frequency content **6**
5.1 Four real coordinates in compact notation 6
5.2 Signed projections, folded petals, and recurrence 7
5.3 Three different comparisons across shapes 8

6 Supporting action, energy, and a response benchmark **8**
6.1 An explicit action supporting the trajectory 8
6.2 Where resonance enters 9

7 Hydrogen reference spectrum and exact identities **9**

8 Exact complete-pattern matches **10**
8.1 Definition and exhaustive finite search 10
8.2 All seven common-rotation placements 10
8.3 All three common-precession placements 11

9 The square sequence already contained in the orbit action **12**
9.1 Exact placements of the square pattern 12

10 Repeated patterns across octaves **13**
10.1 What creates further repetitions 15

11 Absolute frequency and division diagnostics **15**
11.1 Ground-scale diagnostic 15
11.2 The power-law curve from repeated division 16

12 From prescribed precession to nuclear dynamics **16**

13 Conclusion **17**

A All 43 square-pattern placements through level 100 **17**

B Constants and units **19**

1 How the investigation developed

The route to the calculation began with a dimensional interpretation of particle masses, rather than with a fitted hydrogen wavelength. In the development of Infinite Dimensional Wave Theory (IDWT), searches for common fundamentals in particle mass-equivalent frequencies led to groups associated with cumulative simplex counts. The resulting working prescription is

$$\nu_{\text{particle}} = C(n,d)\nu_{0,\mathcal{P}}, \qquad C(n,d) = \binom{n+d-1}{d}, \qquad n \geq 1. \tag{1}$$

The count follows a hockey-stick identity: summing successive layer counts gives a higher cumulative binomial count. In this prescription d classifies the number of bound spatial directions involved in a particle pattern; $\nu_{0,\mathcal{P}}$ is a fundamental associated with a kind of pattern. This formula is the motivating background, not an equation of electron translation. Its parameters and assignments were developed using known particle data. The present calculation does not rederive those masses.

The working assignments place photons at depth two, down-type quarks at three, up-type quarks at four, neutrinos at five, electron/muon patterns at six, and the tau at ten. These are literal spatial directions within one containing space, with further directions unbound. In particular, the electron is a depth-six object, while its proposed external motion around a nucleus uses four real spatial coordinates. This distinction motivated asking whether familiar projected atomic shapes could come from actual higher-dimensional trajectories.

An existing rotation-plus-precession construction supplied a concrete trajectory. Its folded projections included two-, four-, and six-petal displays. Rather than treating a picture alone as a model of spectroscopy, the next question was what frequencies the complete trajectory contains. The decomposition into $|\delta - \beta|$ and $\delta + \beta$ followed directly from its equation. Integer precession/rotation ratios then produced simple component-frequency ratios. This made hydrogen spectroscopy a quantitative comparison rather than solely a visual analogy.

The initial optical question concerned selective interaction with polarized light: might a moving electron react strongly to light matching its motion, leaving a deficit in the transmitted spectrum? That question differs from assuming that an unperturbed orbit continuously emits every frequency it contains. The frequency calculation itself does not decide the strength, polarization dependence, or net direction of energy transfer.

The absolute-scale test came next. The electron mass, the hydrogen binding energy scale, and the Bohr length were supplied to the speed and orbit equations. No wavelength was adjusted. The lower four-petal component came out at about 2.94×10^{15} Hz, or 101.91 nm: ultraviolet, near Lyman-β. This is a conditional absolute output from atomic energy and length inputs, not a fit to that line. The specific energy/radius identifications and the residual difference are retained below.

The investigation then moved from individual coincidences to whole patterns. Division tests suggested comparing repeated copies across the spectrum. The stronger formulation demanded one scale for every component of an entire orbit-frequency pattern. Exact rational searches found the seven common-rotation placements and the octave chain described below. A subsequent comparison exposed the square pattern $(1, 4, 9, 16)$; tracing it back through the same equations identified it as the total-energy sequence at fixed mass, radius, and rotation rate. Its 43 level-100 placements and 147 level-200 placements are included in full.

Some exploratory constructions and numerical settings required trial and error. The main development presented here follows the surviving equations and reproducible results. Superseded numerical attempts remain in the archive. Limits that still affect the current interpretation are stated alongside the results, rather than hidden in that history.

2 Distinctions from earlier atomic models

The use of a literal electron trajectory is not itself new. Bohr used definite electron orbits, Sommerfeld extended old quantum theory to additional periodic motions and relativistic precession, and classical electrodynamic approaches have investigated driven atomic motion. The distinctions concern the proposed geometry, the physical frequency identification, and the route to selection, not priority for orbits or resonance in general.

1. **Four real spatial coordinates for external motion.** The proposed orbit moves through four spatial directions; its precession is not merely rotation of a planar ellipse's periapsis. The electron's depth-six field structure is distinct from its external trajectory.

2. **A particle-dimensional motivation.** The spatial-depth picture precedes the hydrogen comparison and originates in the mass/count program. This is a shared motivating geometry; the mass formula by itself does not derive the atomic action or orbit size.

3. **Mechanical component resonance as a testable hypothesis.** Bohr's spectral frequency is an energy difference divided by h, generally different from either orbit's revolution frequency. His correspondence argument relates them in an appropriate high-level limit. Here direct response at $|\delta \pm \beta|$ is examined explicitly. The supplied driven action has those poles; its identification with physical hydrogen response remains a further step [1].

4. **An absolute diagnostic without wavelength tuning.** The ultraviolet component is calculated from stated atomic energy and length inputs. The later whole-pattern searches select scales from the line set and are explicitly a different comparison protocol.

5. **Whole-pattern and octave comparisons.** The calculation preserves all components under one common scale, and lists every exact assignment within declared bounds. The known Rydberg scaling law explains dependencies between repetitions. Repetition is not claimed as a new property of the Rydberg formula or a calibrated probability.

6. **Nuclear dimensional asymmetry as a candidate precession source.** The trial potential distinguishes a four-direction attractive contribution from a three-direction repulsive contribution. The resulting precession is conditional on that force prescription; this differs from introducing precession solely as a relativistic correction to a central planar orbit.

Bohr supplies a stronger completed hydrogen benchmark than a trajectory picture alone: given his quantization postulates, he obtains the gross bound-state energies and spectral scale. The present program has not yet obtained the corresponding selected atomic states from its full dynamics. These differences specify the intended research approach, not a claim that all of its ingredients are unprecedented or that it supersedes the empirical successes of quantum mechanics.

3 The question and the result

Hydrogen offers a precise test of any proposed electron motion: can the frequencies of that motion account for the frequencies at which hydrogen interacts with light? The construction studied here begins with a literal precessing trajectory, not a probability distribution for electron position. Its component frequencies depend on an integer ratio between two angular rates. The central question is whether the resulting *complete patterns*, rather than isolated ratios, occur repeatedly among hydrogen lines.

The main result is an exact correspondence. For example, the four transitions

$$20 \to 10, \qquad 40 \to 8, \qquad 5 \to 4, \qquad 10 \to 5 \tag{2}$$

have gross frequencies

$$\frac{3}{400} cR_H \, (1, 2, 3, 4). \tag{3}$$

That is precisely the normalized frequency pattern obtained from three members of the orbit family at a common rotation rate. All four components match simultaneously: there is one common frequency scale, not four independently adjusted peaks. Six other exact scales occur through upper principal level 100. Four successive octave placements occur through level 200. Tables and proofs below make these statements directly checkable.

The reference equation is the nonrelativistic, reduced-mass gross hydrogen spectrum. "Exact" throughout the exact searches means equality in that equation, evaluated with rational arithmetic. It does not mean that every fine-structure-resolved laboratory line obeys the gross equation exactly. The exact tables below use that gross-spectrum convention. The line frequencies are the actual target quantities in the comparison; no artificial frequency distance is inserted between a pattern component and its exact match.

The physical proposal is that hydrogen can realize members of this orbit family under appropriate conditions, with resonant interaction at their component frequencies. The presence of matching spectral frequencies is consistent with that proposal, but does not by itself identify the underlying motion. In particular, the complete-pattern tables compare transitions across different hydrogen preparations. They are not a claim that one atom in one initial state simultaneously supports every listed trajectory.

This paper develops the successful correspondences from their equations. It does not attempt to establish the entire IDWT particle theory. The orbit's dimensional premise, its frequency identities, their embedding in hydrogen's spectrum, and the remaining interaction problem are kept explicit so that each can be assessed separately.

4 Physical scope and notation

Infinite Dimensional Wave Theory (IDWT) proposes a single field on ordinary physical space with infinitely many spatial directions and one time direction. Matter patterns involve up to ten bound spatial directions, with other directions unbound. In the working particle assignments the electron is a six-depth pattern. The external electron motion considered here uses four real spatial coordinates relative to the nucleus; four is not a count of spacetime coordinates. This does not eliminate the electron's remaining spatial structure or impose a lower-dimensional position constraint on it.

Only the explicit four-coordinate motion enters the present calculation. The complete electron–nucleus field, its contact boundary conditions, and the reciprocal interaction with light are not solved here. The project premise retains finite propagation of changes in mutual influence. Neither complex notation nor time averaging supplies an additional physical manifold or a probabilistic electron-position law.

No equality between L and the hydrogen principal quantum number is assumed. The orbit frequency is also distinct from the internal portion/count frequency used in the IDWT mass formula. The symbols u, l in a transition label specify the upper and lower levels; the same positive transition frequency can be used in absorption or emission comparisons without assuming identical physical preparation or line strength.

Table 1: Notation. Orbit labels, hydrogen level labels, and particle mass-count labels are distinct.

Symbol	Meaning	Units
$\mathbf{q}(t)$	Four-coordinate external position	m
r	Constant full trajectory radius	m
β	Angular rotation rate	rad/s
δ	Angular precession rate	rad/s
$L = \delta/\beta$	Chosen integer orbit ratio	dimensionless
$P = 2L$	Petals in the folded display	count
v	Speed along the full trajectory	m/s
ω, ν	Angular and ordinary frequency, $\omega = 2\pi\nu$	rad/s, Hz
k	Supplied restoring coefficient	s^{-2}
K, U, H	Kinetic, potential, total mechanical energy	J
u, l, N	Hydrogen principal-level labels	integers
s	Common scale of a frequency-pattern placement	Hz
R_H	Reduced-mass hydrogen Rydberg constant	m^{-1}

5 The trajectory and its exact frequency content

5.1 Four real coordinates in compact notation

Group the real coordinates into two complex numbers solely as a notational convenience:

$$\mathbf{z}(t) = re^{\mathrm{i}\beta t}\begin{pmatrix}\cos\delta t\\ \sin\delta t\end{pmatrix}, \qquad \mathbf{q} = (\Re z_1, \Im z_1, \Re z_2, \Im z_2). \tag{4}$$

With $\delta = L\beta$ and $\theta = \beta t$, this is explicitly

$$\frac{\mathbf{q}(t)}{r} = \begin{pmatrix}\cos L\theta\cos\theta\\ \cos L\theta\sin\theta\\ \sin L\theta\cos\theta\\ \sin L\theta\sin\theta\end{pmatrix}. \tag{5}$$

The sum of the four squared entries is one, so the full radius remains r. An apparent approach to the center in a projection need not be an approach to the center in the full four-coordinate motion.

Proposition 5.1 (Component frequencies and speed)**.** *The trajectory has two circular components, with angular-frequency magnitudes $|\beta - \delta|$ and $\beta + \delta$ for $\beta, \delta \geq 0$. Its speed satisfies*

$$v^2 = r^2(\beta^2 + \delta^2). \tag{6}$$

Proof. The orthogonal transformation of the four real coordinates represented by

$$\zeta_- = \frac{z_1 - \mathrm{i}z_2}{\sqrt{2}} = \frac{r}{\sqrt{2}}e^{\mathrm{i}(\beta-\delta)t}, \qquad \zeta_+ = \frac{z_1 + \mathrm{i}z_2}{\sqrt{2}} = \frac{r}{\sqrt{2}}e^{\mathrm{i}(\beta+\delta)t} \tag{7}$$

exhibits both circular components. Their squared speeds sum to $r^2[(\beta-\delta)^2 + (\beta+\delta)^2]/2$, which is Eq. (6). □

For integer $L \geq 1$,

$$\omega_- = (L-1)\beta, \quad \omega_+ = (L+1)\beta, \quad \frac{\omega_+}{\omega_-} = \frac{L+1}{L-1} \quad (L > 1). \tag{8}$$

Thus $L = 2, 3, 4$ give $3:1$, $2:1$, and $5:3$. At $L = 1$ one component is static; zero frequency is excluded from optical pattern searches.

5.2 Signed projections, folded petals, and recurrence

The signed first-plane projection is

$$z_1 = r\cos(L\theta)e^{i\theta}. \tag{9}$$

Its distinct petals number L for odd L and $2L$ for even L; the $L = 1$ case is an offset circle. The visualization convention replaces the signed radial coordinate by $|\cos L\theta|$, producing $2L$ folded petals. Consequently the familiar two-, four-, and six-petal displays refer to $L = 1, 2, 3$ under this folded convention. Folding changes the display and must not be mistaken for another equation of motion. Figure 1 shows both versions.

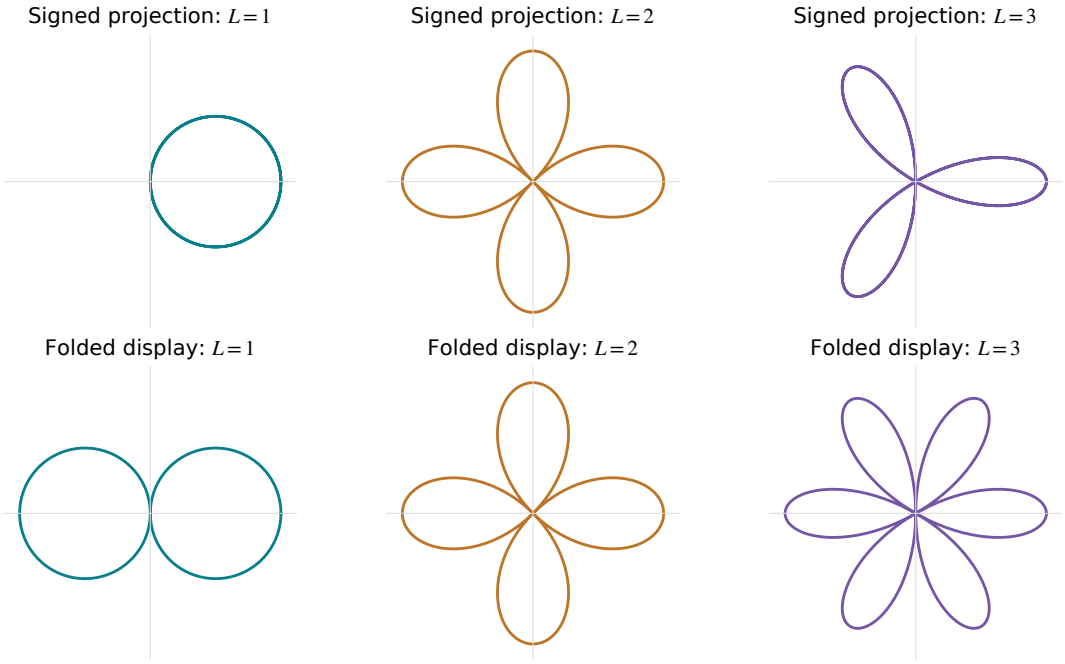


Figure 1: Top: signed projections of Eq. (4). Bottom: the folded visualization convention giving two, four, and six petals. The full trajectory has constant radius in four real spatial coordinates. The bottom row illustrates the display labels; it does not replace the signed motion.

Position and velocity recur at

$$T = \frac{2\pi}{\beta\ \gcd(L-1, L+1)}. \tag{10}$$

This follows by demanding recurrence of both circular phases. The greatest common divisor is two for odd L and one for even L. Recurrence of this prescribed trajectory does not prove recurrence of an independently evolving nuclear field. Likewise, a petal count alone is not a frequency conversion.

For a projected combination $Z = \cos\chi\,\zeta_- + \sin\chi\,\zeta_+$,

$$|Z|^2 = \frac{r^2}{2}\left[1 + \sin(2\chi)\cos(2\delta t)\right]. \tag{11}$$

Projection changes component weights; a nonlinear observable such as squared radius can contain a new combination frequency. Identifying such an observable with optical interaction requires a response law.

5.3 Three different comparisons across shapes

At fixed speed and radius, Eq. (6) gives

$$\beta = \frac{v}{r\sqrt{1+L^2}}, \qquad \nu_\pm = \frac{(L\pm 1)v}{2\pi r\sqrt{1+L^2}}. \tag{12}$$

This is different from holding β fixed, and different again from holding δ fixed. In the last case $\beta = \delta/L$ and $\omega_\pm = \delta(1 \pm 1/L)$. The denominator is L only under that specified comparison; at fixed v, r it is $\sqrt{1+L^2}$.

For $L = 1, 2, 3$, merge equal frequencies, remove zero, and normalize by the lowest nonzero frequency. The three patterns are

$$A = (1, 2, 3, 4) \qquad \text{at fixed } \beta, \tag{13}$$

$$B = (1, 4/3, 8/3, 3, 4) \qquad \text{at fixed } \delta, \tag{14}$$

$$C = (1, \sqrt{2}, 2\sqrt{2}, 3, \sqrt{10}) \qquad \text{at fixed } v, r. \tag{15}$$

For example, the unnormalized common-β components are $(0,2)\beta$, $(1,3)\beta$, and $(2,4)\beta$. Their distinct positive union gives A. These are families of alternative prepared motions, not independently postulated physical modes cohabiting one electron.

6 Supporting action, energy, and a response benchmark

6.1 An explicit action supporting the trajectory

Let $J = \mathrm{diag}(J_2, J_2)$ with $J_2(x, y) = (-y, x)$. A supplied quadratic action is

$$\mathcal{L} = \frac{m}{2}|\dot{\mathbf{q}}|^2 + m\beta\mathbf{q}^T J\dot{\mathbf{q}} - \frac{mk}{2}|\mathbf{q}|^2. \tag{16}$$

Since $J^T = -J$, its Euler–Lagrange equation is

$$\ddot{\mathbf{q}} = 2\beta J\dot{\mathbf{q}} - k\mathbf{q}, \qquad k = \delta^2 - \beta^2. \tag{17}$$

Direct differentiation verifies Eq. (4). This gives a concrete dynamical realization of the prescribed kinematics. It does not derive the coefficients from an electron–nucleus field solution, nor show that all values of L are selected by one unchanged physical interaction.

The conserved mechanical energy contains no contribution from the term linear in velocity:

$$K = \frac{mr^2}{2}(\delta^2 + \beta^2), \qquad U = \frac{mr^2}{2}(\delta^2 - \beta^2), \qquad H = mr^2\delta^2. \tag{18}$$

At fixed r, δ,

$$\frac{K}{H} = \frac{1}{2}\left(1 + \frac{1}{L^2}\right), \quad \frac{U}{H} = \frac{1}{2}\left(1 - \frac{1}{L^2}\right), \quad \frac{k}{\delta^2} = 1 - \frac{1}{L^2}. \tag{19}$$

The inverse-square form is exact and resembles the hydrogen level formula. Its role matters: k has units s^{-2}, so this dimensionless coefficient is not itself an optical frequency. Moreover H is constant in this comparison. For two labels $a < b$,

$$\frac{U_b - U_a}{H} = \frac{1}{2}\left(\frac{1}{a^2} - \frac{1}{b^2}\right), \qquad K_b - K_a = -(U_b - U_a), \qquad H_b - H_a = 0. \tag{20}$$

An energy difference assigned only to U is therefore not the total energy released between these preparations. Changing L at fixed δ also changes β and k in the prescribed action.

6.2 Where resonance enters

An explicitly external electromagnetic benchmark supplies a force

$$\ddot{\mathbf{q}} = 2\beta J\dot{\mathbf{q}} - k\mathbf{q} + \frac{\mathbf{F}(t)}{m}, \quad \mathbf{F}(t) = -eE_0\boldsymbol{\epsilon}\cos(\omega t + \phi). \tag{21}$$

Here $\boldsymbol{\epsilon}$ is a specified spatial projection of the drive polarization. No absolute IDWT field amplitude is inferred from E_0. For the two circular polarizations the inverse-response denominators are

$$D_\pm(\omega) = k - \omega^2 \pm 2\beta\omega. \tag{22}$$

Their positive roots for $\delta > \beta$ are $\delta + \beta$ and $\delta - \beta$. Thus the component frequencies are also resonance frequencies of this supplied linear law. In contrast, $1 - 1/L^2$ does not replace these poles. Orientation can change the weights exciting the two circular components; calculating the full light–atom polarization response requires the actual field coupling and reciprocal dynamics.

Resonance can produce strong interaction at selected incident frequencies, potentially leaving a deficit in transmitted light. A finite transmission curve requires energy accounting, line widths, saturation or damping where physically appropriate, and a definition of what the detector measures. The undamped denominator alone is not a finite absorption coefficient. The mechanical work in the benchmark is

$$W = \int \mathbf{F}(t) \cdot \dot{\mathbf{q}}(t)\, dt. \tag{23}$$

The empirical photon energy relation is $E_\gamma = h\nu$. A constant energy transfer would imply a constant frequency change, while a constant fractional frequency change would require a transfer proportional to $h\nu$. The division tests below do not calculate either backreaction law.

7 Hydrogen reference spectrum and exact identities

The reference frequencies are

$$\nu_{ul} = cR_H\left(\frac{1}{l^2} - \frac{1}{u^2}\right), \qquad u > l \geq 1, \tag{24}$$

where $R_H = R_\infty\mu/m_e$ and $\mu = m_e m_p/(m_e + m_p)$. The inverse-square hydrogen series provides the gross-spectrum comparator [6]. Fine structure, Lamb shifts, and hyperfine structure are outside Eq. (24). Catalog wavelengths are handled separately; the NIST hydrogen table distinguishes resolved fine components from unresolved multiplet values [4].

Define the finite set of distinct dimensionless frequencies

$$\mathcal{F}_M = \left\{ \frac{1}{l^2} - \frac{1}{u^2} : 1 \le l < u \le M \right\}. \tag{25}$$

There are $M(M-1)/2$ transition assignments before merging exactly equal frequencies. Pair counts below count transition assignments, while pattern placement counts count distinct frequency scales. The distinction handles degeneracies explicitly.

Two useful identities are

$$\nu_{ac} = \nu_{ab} + \nu_{bc} \qquad (a > b > c), \tag{26}$$

$$\nu_{ku,kl} = \frac{\nu_{ul}}{k^2} \qquad (k \in \mathbb{N}). \tag{27}$$

The first is the Ritz combination relation; the second follows by factoring k^{-2} from Eq. (24). Both are direct algebraic identities. Common index doubling gives a frequency division by four: *two* octaves, not one. All ratios in the gross spectrum are rational.

For orientation, exact pair examples are

$$\frac{\nu_{32}}{\nu_{63}} = \frac{5}{3}, \qquad \frac{\nu_{53}}{\nu_{15,5}} = 2, \qquad \frac{\nu_{15,3}}{\nu_{15,5}} = 3. \tag{28}$$

The full-pattern results impose all component ratios together and are therefore more specific than checking these pairs separately.

8 Exact complete-pattern matches

8.1 Definition and exhaustive finite search

A normalized pattern $T = (t_1, \ldots, t_p)$, $t_1 = 1$, has an exact placement at dimensionless scale $\sigma = s/(cR_H)$ when

$$\sigma t_i \in \mathcal{F}_M \quad \text{for every } i. \tag{29}$$

Because $t_1 = 1$, every exact scale must itself be in $\mathcal{F}_M$. Enumerating each member of $\mathcal{F}_M$ and testing Eq. (29) is therefore exhaustive within the declared upper-level bound. Fractions are reduced exactly; no numerical tolerance defines the exact counts.

For approximate placements, the same anchored procedure chooses the nearest reference frequency to each predicted component under relative error and requires distinct chosen frequencies. The reported score is

$$\varepsilon_{\max} = \max_i \left| \frac{s t_i}{\nu_i^{\text{match}}} - 1 \right|. \tag{30}$$

The lowest component remains exactly anchored to a reference line. This is not a continuous optimization of the common scale, nor a global search over all possible injective near-line assignments when nearest choices coincide. These qualifications affect approximate controls, not the exhaustive exact membership test.

8.2 All seven common-rotation placements

Table 3 lists every exact A placement through $M = 100$. Each entry gives an upper-to-lower transition. Any row can be verified directly by inserting its indices into Eq. (24). For the example

Table 2: Complete-pattern results. Percentages describe the best eligible anchored C placement; A and B entries count exact scales.

Upper level M	Exact A	Exact B	Best C error
10	0	0	1.82338%
20	0	0	0.551724%
40	2	0	0.105594%
100	7	3	0.00463128%
200	20	10	not searched here

in the introduction,

$$\frac{1}{10^2}-\frac{1}{20^2}=\frac{3}{400}, \qquad \frac{1}{8^2}-\frac{1}{40^2}=\frac{6}{400}, \tag{31}$$

$$\frac{1}{4^2}-\frac{1}{5^2}=\frac{9}{400}, \qquad \frac{1}{5^2}-\frac{1}{10^2}=\frac{12}{400}. \tag{32}$$

These are exact line-frequency equalities, not merely nearby locations.

Table 3: All exact $(1,2,3,4)$ placements with $u \le 100$.

$s/(cR_H)$	s	$2s$	$3s$	$4s$
5/7056	$42 \to 28$	$56 \to 24$	$84 \to 21$	$21 \to 14$ or $63 \to 18$
2/2025	$90 \to 30$	$30 \to 18$	$90 \to 18$	$45 \to 15$
1/900	$40 \to 24$	$60 \to 20$	$30 \to 15$	$20 \to 12$
3/1600	$40 \to 20$	$80 \to 16$	$10 \to 8$	$20 \to 10$
1/450	$60 \to 20$	$20 \to 12$	$60 \to 12$	$30 \to 10$
3/400	$20 \to 10$	$40 \to 8$	$5 \to 4$	$10 \to 5$
2/225	$30 \to 10$	$10 \to 6$	$30 \to 6$	$15 \to 5$

The seven scales produce eight transition assignments because the first row has two alternatives at its highest frequency. Dividing all indices within each assignment by their common greatest common divisor leaves five distinct index assignments. This records one source of repetition; it does not establish statistical independence between the remaining assignments. The $s = 3cR_H/400$ placement also extends to $(1,2,3,4,5)$ by adding $20 \to 5$ at $5s$.

8.3 All three common-precession placements

The five-component pattern B also occurs exactly. Its three scales through $M = 100$ are shown in Table 4. They remain distinct after common integer scaling of transition indices is removed.

Table 4: All exact $(1, 4/3, 8/3, 3, 4)$ placements with $u \le 100$.

$s/(cR_H)$	s	$4s/3$	$8s/3$	$3s$	$4s$
5/9408	$24 \to 21$	$42 \to 28$	$56 \to 24$	$84 \to 24$	$84 \to 21$
1/1200	$60 \to 30$	$40 \to 24$	$60 \to 20$	$15 \to 12$	$30 \to 15$
2/675	$90 \to 18$	$45 \to 15$	$15 \to 9$	$30 \to 10$	$45 \to 9$

Proposition 8.1 (The fixed-speed distinction)**.** *The complete pattern C cannot have an exact placement in the gross Rydberg spectrum at any nonzero common scale.*

Proof. Two of its components have ratio $\sqrt{2}$. The ratio of any two nonzero frequencies in Eq. (24) is rational. The common scale cancels from the ratio, giving a contradiction. □

Approximate placements of C are possible and become closer as the search range grows. This distinguishes the three preparations mathematically. It does not alone determine which quantity nature holds fixed across orbit shapes, nor exclude effects absent from the gross reference equation.

9 The square sequence already contained in the orbit action

The sequence $(1, 4, 9, 16)$ has a direct origin in the same orbit family. It must therefore be considered alongside the linear component-frequency patterns, rather than classified solely as an unrelated control. Since $\delta_L = L\beta$ and $H_L = mr^2\delta_L^2$,

$$\frac{H_L}{mr^2\beta^2} = L^2, \qquad L = 1, 2, 3, 4. \tag{33}$$

In this fixed-β comparison the supporting coefficient also changes as $k_L = (L^2 - 1)\beta^2$. The square energies therefore compare members of the supplied action family, rather than selected states of one fixed-k Hamiltonian. Here mass, full radius, and rotation rate are held fixed. Equivalently, $\delta_L^2/\beta^2 = L^2$. Thus the square sequence is an exact total-energy sequence of the supplied action family under this comparison. It is distinct from the earlier fixed-precession comparison, where the total energy stays constant.

The two component rates give the same identity:

$$\left(\frac{\omega_+ + \omega_-}{2\beta}\right)^2 = L^2. \tag{34}$$

The linear response poles themselves remain $(L \pm 1)\beta$. Reading Eq. (33) as four optical frequencies requires a physical energy-transfer identification. If one introduces the energy-equivalent frequency H_L/h, its ratios are exactly $1 : 4 : 9 : 16$, with common scale $mr^2\beta^2/h$. This conversion does not establish which energy transfers are allowed or whether a photon couples to total energy, an energy difference, or a component of the motion. Differences at fixed m, r, β satisfy

$$H_b - H_a = mr^2\beta^2(b^2 - a^2). \tag{35}$$

These square differences differ from the inverse-square hydrogen level differences. Neither equality of pattern ratios nor a change of notation supplies the missing physical map.

9.1 Exact placements of the square pattern

Apply the same whole-pattern definition to $Q = (1, 4, 9, 16)$, with one common scale and no independent peak adjustments. The exact search reported 43 distinct exact scales through upper level 100 and 147 through level 200. A fresh principal fraction-based enumeration reproduces both counts. Every scale and all transition alternatives are supplied in `square-pattern-checks.json`. Appendix A lists one complete assignment at each of the 43 level-100 scales.

Pattern	Exact scales, $M = 100$	Exact scales, $M = 200$
$A = (1, 2, 3, 4)$	7	20
$B = (1, 4/3, 8/3, 3, 4)$	3	10
$Q = (1, 4, 9, 16)$	43	147

The square pattern has more exact placements under the declared bounds. Counts alone are not a calibrated comparison of physical models: the patterns have different spacings, share lines and scaled copies, and were examined during an exploratory investigation. The result establishes that an additional sequence already present in the orbit action repeatedly embeds in the gross hydrogen spectrum. It makes the choice of physical observable central: linear motion, squared rate, and total energy have different roles even when all arise from the same trajectory.

10 Repeated patterns across octaves

An octave is a factor of two in frequency. A chain of b complete pattern placements requires

$$2^j \sigma t_i \in \mathcal{F}_M \quad \text{for every } i \text{ and } j = 0, \ldots, b-1. \tag{36}$$

Shared components of adjacent blocks are counted as shared frequencies. For A, the union of four blocks is

$$s\,(1, 2, 3, 4, 6, 8, 12, 16, 24, 32), \qquad s = \frac{cR_H}{3600}. \tag{37}$$

There are ten distinct frequencies, not sixteen independent observations.

Table 5: Exact octave-chain counts, classified by starting scale. A longer chain can contain shorter chains.

Pattern	M	Single placements	Two blocks	Three blocks	Four blocks
A	100	7	1	0	0
B	100	3	0	0	0
A	200	20	4	2	1
B	200	10	0	0	0

The four-block chain uses scales cR_H times 1/3600, 1/1800, 1/900, and 1/450. Table 6 provides one exact transition assignment for every component of every block. Its rows are generated by the standalone fraction checker, not by rounding frequencies to visually attractive positions.

Table 6: Explicit assignments for the four consecutive octave blocks. Within each row the frequency pattern is $(1, 2, 3, 4)$ times that row's scale.

Row scale/(cR_H)	First	Second	Third	Fourth
$\frac{1}{3600}$	$45 \to 36$	$120 \to 40$	$60 \to 30$	$40 \to 24$
$\frac{1}{1800}$	$120 \to 40$	$40 \to 24$	$120 \to 24$	$60 \to 20$
$\frac{1}{900}$	$40 \to 24$	$60 \to 20$	$30 \to 15$	$20 \to 12$
$\frac{1}{450}$	$60 \to 20$	$20 \to 12$	$60 \to 12$	$30 \to 10$

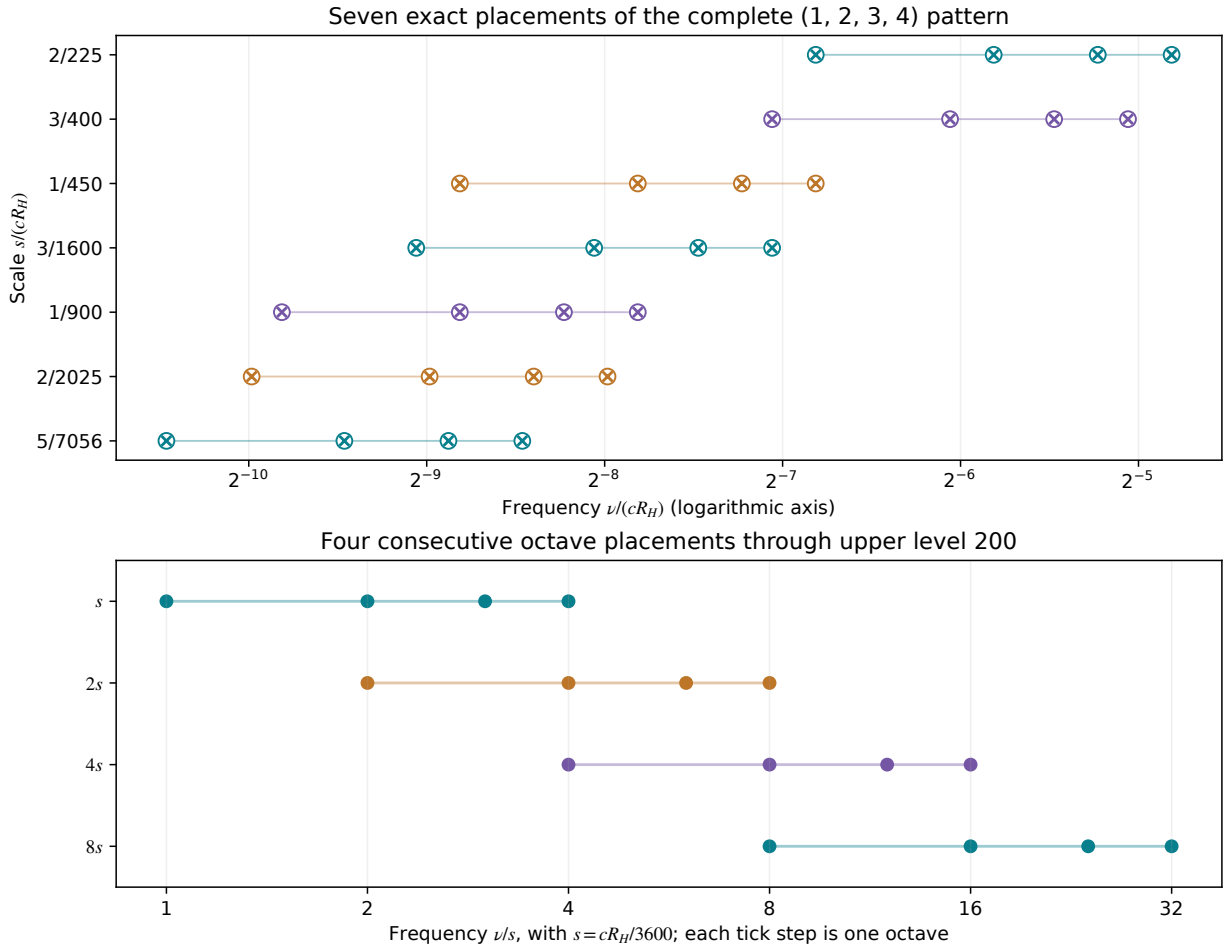


Figure 2: Top: all seven exact common-rotation placements through level 100. Crosses mark orbit-pattern frequencies and open circles mark the matched gross hydrogen frequencies; they coincide. Bottom: the four complete blocks at octave-separated scales through level 200. Horizontal spacing is logarithmic. Vertical placement separates comparisons and does not encode line intensity.

10.1 What creates further repetitions

Corollary 10.1 (Lower-frequency copies and octave continuation)**.** *An exact complete-pattern placement has copies at every scale divided by an integer square. If placements occur at both s and $2s$, then the unbounded gross spectrum contains consecutive octave placements $2s, s, s/2, s/4, s/8, \ldots$.*

Proof. Multiply all indices of an assignment by k and apply Eq. (27). In particular, repeated doubling gives placements at $s/4^j$ and $2s/4^j$. The union of these two sequences covers every successive descending octave. □

This exposes a dependency in the finite result: the placements at $cR_H/900$ and $cR_H/450$ already generate those at $cR_H/3600$ and $cR_H/1800$ by doubling their indices. The four-block chain is a genuine exact match, but its four blocks are not four separate arithmetic surprises. At fixed M the available index range limits the continuation. In the unbounded ideal formula the continuation follows mathematically; its experimental population and observability are separate questions.

No adjacent B octave chains occur in the searched ranges. That is a bounded enumeration, not a theorem excluding them at higher levels.

11 Absolute frequency and division diagnostics

The exact pattern searches determine allowed common scales *from the hydrogen frequency set.* They do not derive those scales from orbit size and speed. A separate diagnostic attempts an absolute calibration using the electron mass, the Bohr length, and the hydrogen binding energy.

11.1 Ground-scale diagnostic

Using CODATA constants [3] and the NIST ionization energy [4], take

$$r = a_0 = 5.29177210544 \times 10^{-11}\,\mathrm{m}, \quad K = 13.598433\,\mathrm{eV}, \quad v = \sqrt{\frac{2K}{m_e}} = 2.187107498 \times 10^{6}\,\mathrm{m/s}. \tag{38}$$

The assignments $r = a_0$ for the full four-coordinate radius and $K = |E_{\mathrm{binding}}|$ are conditional. The latter is a conventional Coulomb virial benchmark, not a derived energy partition of Eq. (16). Equation (12) then gives Table 7.

Table 7: Absolute-clock diagnostic at fixed v, r. Wavelength means c/ν; an emission or absorption strength has not been calculated.

L	ν_- (10^{15} Hz)	ν_+ (10^{15} Hz)	λ_- (nm)	λ_+ (nm)
2	2.941738920	8.825216759	101.909947	33.969982
3	4.160247077	8.320494154	72.061215	36.030607
4	4.786145780	7.976909633	62.637553	37.582532

The $L = 2$ lower component lies near Lyman-β, with frequency about 0.64986% above the selected NIST catalog value at 102.57222 nm. The other five components have $h\nu$ above the ground-state ionization energy and cannot be bound-to-bound line frequencies under this calibration. This does not test continuum interaction. A fixed-nucleus Coulomb energy $K = hcR_\infty$ gives 101.882754 nm, while a consistent reduced-mass relative-coordinate control gives 101.938241 nm. Neither removes the gap.

The fixed-nucleus benchmark has

$$\frac{v}{2\pi a_0} = 2cR_\infty, \qquad \frac{\nu_\pm}{cR_\infty} = \frac{2(L \pm 1)}{\sqrt{1+L^2}}. \tag{39}$$

Consequently an ultraviolet atomic scale is expected from these supplied hydrogen energy and length inputs. Its appearance is not by itself an independent frequency prediction.

11.2 The power-law curve from repeated division

Let $\nu_0 = 2.941738919617216 \times 10^{15}\,\mathrm{Hz}$ and $\lambda_0 = c/\nu_0 = 101.9099472087$ nm, from the absolute $L = 2$ calculation. Repeated division by four gives $D = 4^j$, $\nu_j = \nu_0/D$, $\lambda_j = D\lambda_0$. Compare the fixed hydrogen family $(3 \cdot 2^j) \to 2^j$. Its frequencies scale in exactly the same way, hence

$$\frac{\nu_j}{\nu_{\mathrm{ref},j}} - 1 = 0.00650995117778, \tag{40}$$

$$\Delta\lambda_j = (\lambda_{\mathrm{ref},0} - \lambda_0)D = 0.6634287809\,\mathrm{nm}\,D. \tag{41}$$

The absolute wavelength gap is a power law of exponent one in D, or exponential in step number j; the fractional frequency error is constant. This is the initial mismatch carried through the common scaling law, not a calculated cumulative perturbation by incident photons.

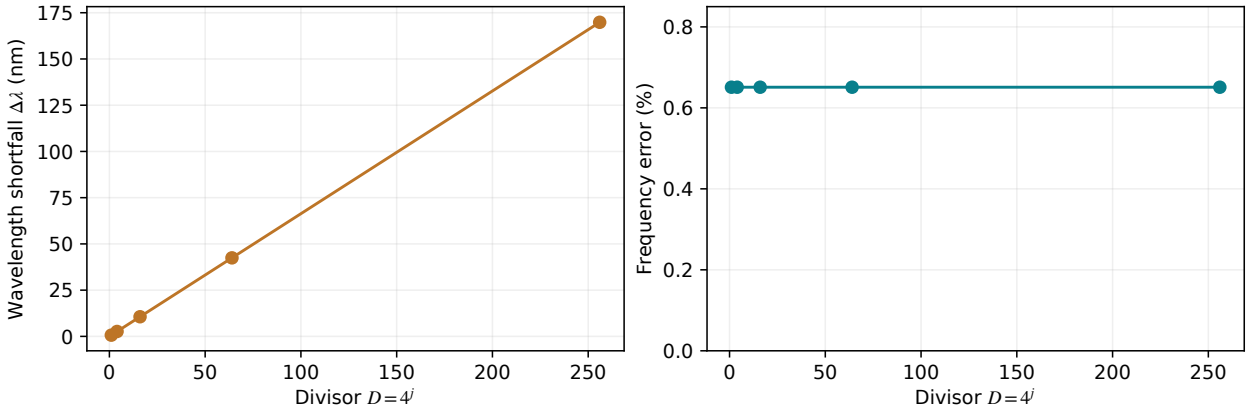


Figure 3: The repeated-division diagnostic. The wavelength gap grows linearly with the divisor, while the fractional frequency error stays fixed. Both curves follow Eq. (41); they do not fit a new interaction law.

12 From prescribed precession to nuclear dynamics

The later numerical work treats the nucleus as a fixed reference initially, with electron coordinate $\mathbf{q} = (x_1, x_2, x_3, w)$ and trial potential

$$V(\mathbf{q}) = -\frac{a}{\rho} + \frac{b}{r_3}, \qquad \rho = |\mathbf{q}|, \quad r_3 = \sqrt{x_1^2 + x_2^2 + x_3^2}. \tag{42}$$

For the proton comparison $(a, b) = (4/3, 1/3)$; the down contribution is repulsive for the electron and independent of w in this trial realization of free extension. Thus

$$\ddot{\mathbf{x}} = -\frac{a\mathbf{x}}{\rho^3} + \frac{b\mathbf{x}}{r_3^3}, \qquad \ddot{w} = -\frac{aw}{\rho^3}. \tag{43}$$

The $1/r$ kernels and coordinate-independent extension are supplied approximations, not derived electromagnetic reduction or a resolved contact boundary problem. Net circular launch speed at $w = 0$ is $v_c = \sqrt{(a-b)/r}$ in the mass-one units. This corrected an earlier launch normalization using only the attractive contribution.

Tilted trajectories in this supplied anisotropic potential exhibit precession, whereas the isotropic case has constant orbital plane. Thus this calculation generates precession from a force law rather than prescribing its rate in the trajectory. The result is conditional on the stated kernels and nuclear geometry; it establishes a candidate source of precession, not integer state selection or a complete electromagnetic hydrogen model.

A separate principal validation recovered exact flat-trajectory ratios $L = 2, \ldots, 6$ and checked six 16-rotation integrations at two tolerances. Tight-run relative energy drift was approximately 7×10^{-10} to 10^{-8}. The current axisymmetric preparation spans at most three linear spatial directions, so its precession is not identified with the complete four-direction target solely from two spectral peaks. The rate pair is also invariant under exchanging the names β and δ; geometry must fix that assignment. These qualifications specify the numerical result being reported.

13 Conclusion

The successful progression connects a particle-dimensional picture to literal electron motion, then to exact frequency and energy structure. The orbit decomposition yields $(L-1)\beta$ and $(L+1)\beta$; the supplied action yields both the inverse-square energy-share identity and the square total-energy sequence under their distinct fixed-quantity comparisons. The ultraviolet calibration follows without wavelength tuning. Whole-pattern searches establish seven common-rotation placements, three common-precession placements, the octave chain, and 43 square-pattern placements through upper level 100. Their equations and assignments are explicit, so the reader can reproduce every exact equality directly.

The dynamical precession result adds a concrete force-based realization of one aspect of the proposed motion. The remaining physical identification is to derive the selected states, absolute scales, and optical response under a common interaction law. Exact placements are equalities within the gross Rydberg spectrum; they are not presented as independent observations or a statistical significance calculation.

Data and verification

The source package contains the complete mathematical derivations, vector figures, exact assignment data, and standalone Python checkers. The original author verifier passed 563 assertions, and the paper checker passed 218. Exact fraction enumeration reproduces the 43 and 147 square placements. Independent scientific assessment of the complete combined physical interpretation remains open. AI tools assisted calculation and manuscript preparation. The canonical research archive retains exploratory history separately; this paper presents the successful results.

A All 43 square-pattern placements through level 100

Each row gives one exact assignment of frequencies $s(1, 4, 9, 16)$. The scale column is $s/(cR_H)$. Additional assignments at degenerate frequencies and all level-200 placements are retained in the JSON evidence.

Scale	s	$4s$	$9s$	$16s$
5/150528	$96 \to 84$	$48 \to 42$	$32 \to 28$	$24 \to 21$
13/254016	$84 \to 72$	$42 \to 36$	$28 \to 24$	$21 \to 18$
1/14400	$90 \to 72$	$45 \to 36$	$30 \to 24$	$40 \to 24$
7/82944	$96 \to 72$	$48 \to 36$	$32 \to 24$	$24 \to 18$
11/129600	$72 \to 60$	$36 \to 30$	$24 \to 20$	$18 \to 15$
15/123904	$96 \to 66$	$48 \to 33$	$32 \to 22$	$88 \to 22$
1/7938	$72 \to 56$	$36 \to 28$	$84 \to 28$	$18 \to 14$
5/37632	$48 \to 42$	$24 \to 21$	$16 \to 14$	$84 \to 21$
1/7350	$84 \to 60$	$42 \to 30$	$28 \to 20$	$21 \to 15$
1/6400	$60 \to 48$	$30 \to 24$	$20 \to 16$	$15 \to 12$
13/76800	$96 \to 60$	$48 \to 30$	$32 \to 20$	$24 \to 15$
5/28224	$84 \to 56$	$42 \to 28$	$84 \to 24$	$21 \to 14$
5/20736	$72 \to 48$	$36 \to 24$	$24 \to 16$	$18 \to 12$
1/3600	$45 \to 36$	$40 \to 24$	$15 \to 12$	$20 \to 12$
11/37632	$84 \to 48$	$42 \to 24$	$28 \to 16$	$21 \to 12$
1/3072	$96 \to 48$	$48 \to 24$	$32 \to 16$	$24 \to 12$
7/20736	$48 \to 36$	$24 \to 18$	$16 \to 12$	$12 \to 9$
1/2352	$84 \to 42$	$42 \to 21$	$28 \to 14$	$84 \to 12$
15/30976	$48 \to 33$	$88 \to 22$	$16 \to 11$	$44 \to 11$
1/2025	$60 \to 36$	$30 \to 18$	$20 \to 12$	$15 \to 9$
2/3969	$36 \to 28$	$18 \to 14$	$42 \to 14$	$9 \to 7$
1/1728	$72 \to 36$	$36 \to 18$	$24 \to 12$	$18 \to 9$
5/7938	$84 \to 36$	$42 \to 18$	$28 \to 12$	$21 \to 9$
55/82944	$96 \to 36$	$48 \to 18$	$32 \to 12$	$24 \to 9$
7/9216	$32 \to 24$	$16 \to 12$	$96 \to 12$	$8 \to 6$
5/5184	$36 \to 24$	$18 \to 12$	$12 \to 8$	$9 \to 6$
1/768	$48 \to 24$	$24 \to 12$	$16 \to 8$	$12 \to 6$
7/4800	$60 \to 24$	$30 \to 12$	$20 \to 8$	$15 \to 6$
1/648	$72 \to 24$	$36 \to 12$	$24 \to 8$	$18 \to 6$
5/3136	$84 \to 24$	$42 \to 12$	$28 \to 8$	$21 \to 6$
5/3072	$96 \to 24$	$48 \to 12$	$32 \to 8$	$24 \to 6$
1/588	$42 \to 21$	$84 \to 12$	$14 \to 7$	$42 \to 6$
7/2304	$16 \to 12$	$8 \to 6$	$48 \to 6$	$4 \to 3$
5/1296	$18 \to 12$	$9 \to 6$	$6 \to 4$	$36 \to 4$
1/192	$24 \to 12$	$12 \to 6$	$8 \to 4$	$6 \to 3$
1/162	$36 \to 12$	$18 \to 6$	$12 \to 4$	$9 \to 3$
5/768	$48 \to 12$	$24 \to 6$	$16 \to 4$	$12 \to 3$
1/150	$60 \to 12$	$30 \to 6$	$20 \to 4$	$15 \to 3$
35/5184	$72 \to 12$	$36 \to 6$	$24 \to 4$	$18 \to 3$
1/147	$84 \to 12$	$42 \to 6$	$28 \to 4$	$21 \to 3$
7/1024	$96 \to 12$	$48 \to 6$	$32 \to 4$	$24 \to 3$
14/2025	$18 \to 10$	$9 \to 5$	$60 \to 4$	$45 \to 3$
5/324	$9 \to 6$	$36 \to 4$	$3 \to 2$	$18 \to 2$

B Constants and units

Table 9: Numerical inputs. Central values are used; no measurement-uncertainty propagation is claimed for the exploratory calibrations.

c	$299792458\,\mathrm{m/s}$ (exact)
h	$6.62607015 \times 10^{-34}\,\mathrm{J\,s}$ (exact)
$1\,\mathrm{eV}$	$1.602176634 \times 10^{-19}\,\mathrm{J}$ (exact)
m_e	$9.1093837139 \times 10^{-31}\,\mathrm{kg}$
m_p	$1.67262192595 \times 10^{-27}\,\mathrm{kg}$
a_0	$5.29177210544 \times 10^{-11}\,\mathrm{m}$
R_∞	$10973731.568157\,\mathrm{m}^{-1}$
Hydrogen ionization energy	$13.598433\,\mathrm{eV}$

Constants are from the CODATA 2022 compilation [3]; the stated ionization energy is the NIST handbook entry [4]. The reduced mass enters R_H as given in the main text. For the air conversion, with w the air wavelength in Å and $x = 10^4/w$, the implemented VALD formula is

$$n_{\mathrm{air}}(w) = 1 + 0.00008336624212083 + \frac{0.02408926869968}{130.1065924522 - x^2} + \frac{0.0001599740894897}{38.92568793293 - x^2}, \tag{44}$$

$$w_{\mathrm{vacuum}} = w\, n_{\mathrm{air}}(w). \tag{45}$$

Air/vacuum conversion and fine-component selection must be applied before comparing catalog ratios at parts-per-million precision.

References

[1] N. Bohr, *The Structure of the Atom*, Nobel lecture (1922). https://www.nobelprize.org/uploads/2018/06/bohr-lecture.pdf.

[2] D. C. Cole and Y. Zou, *Quantum Mechanical Ground State of Hydrogen Obtained from Classical Electrodynamics* (2003). https://arxiv.org/abs/quant-ph/0307154.

[3] NIST, *CODATA Recommended Values of the Fundamental Physical Constants: 2022*, NIST SP 961 (May 2024). https://physics.nist.gov/cuu/pdf/wall_2022.pdf.

[4] NIST Physical Measurement Laboratory, *Atomic Data for Hydrogen (H)*. https://physics.nist.gov/PhysRefData/Handbook/Tables/hydrogentable1.htm.

[5] NIST Physical Measurement Laboratory, *Strong Lines of Hydrogen (H)*. https://physics.nist.gov/PhysRefData/Handbook/Tables/hydrogentable2_a.htm.

[6] NIST, *Atomic Spectroscopy: Term Series, Quantum Defects*. https://www.nist.gov/pml/atomic-spectroscopy-compendium-basic-ideas-notation-data-and-formulas/atomic-spectroscopy-term.

[7] NIST, *Atomic Spectra Database: Spectral Lines Help*. https://physics.nist.gov/PhysRefData/ASD/Html/lineshelp.html.

[8] VALD documentation, *Wavelength conversion air–vacuum*, inverse conversion attributed to N. Piskunov. https://www.astro.uu.se/valdwiki/Air-to-vacuum%20conversion.